

1      **Molecular Composition and Photochemical Evolution of Water**  
2      **Soluble Organic Carbon (WSOC) Extracted from Field Biomass**  
3      **Burning Aerosols using High Resolution Mass Spectrometry**

4  
5      Jing Cai<sup>1,2</sup>, Xiangying Zeng<sup>1</sup>, Guorui Zhi<sup>3</sup>, Sasho Gligorovski<sup>1</sup>, Guoying Sheng<sup>1</sup>,  
6                  Zhiqiang Yu<sup>1,\*</sup>, Xinming Wang<sup>1</sup>, Ping'an Peng<sup>1</sup>

7  
8      *<sup>1</sup>State Key Laboratory of Organic Geochemistry, Guangdong Key Laboratory of*  
9      *Environment and Resources, Guangzhou Institute of Geochemistry, Chinese*  
10      *Academy of Sciences, Guangzhou, 510640, China*

11      *<sup>2</sup>University of Chinese Academy of Sciences, Beijing, 100049, China*

12      *<sup>3</sup>State Key Laboratory of Environmental Criteria and Risk Assessment, Chinese*  
13      *Research Academy of Environmental Sciences, Beijing, 100012, China*

14  
15      \*corresponding author: Dr. Zhiqiang Yu

16      Tel: +86-13728068752

17      Fax: +86-20-85290288

18      E-mail: zhiqiang@gig.ac.cn

19

20

21

22

23

24

25 **ABSTRACT**

26 Photochemistry plays an important role in the evolution of atmospheric water soluble  
27 organic carbon (WSOC), which dissolves into clouds, fogs and aerosol liquid water. In  
28 this study, we tentatively examined the molecular composition and evolution of a  
29 WSOC mixture extracted from field-collected wheat straw burning aerosol (WSBA)  
30 samples upon photolysis, using direct infusion electrospray ionization (ESI) coupled to  
31 high-resolution mass spectrometry (HRMS) and liquid chromatography (LC) coupled  
32 with HRMS. For comparison, two typical phenolic compounds (i.e., phenol and  
33 guaiacol) emitted from lignin pyrolysis in combination with hydrogen peroxide (H<sub>2</sub>O<sub>2</sub>)  
34 as a typical OH radical precursor were simultaneously exposed to simulated sunlight  
35 irradiation. Their photochemical products such as phenolic dimers (e.g., m/z 185.0608  
36 for phenol dimer and m/z 245.0823 for guaiacol dimer) or their isomers, were also  
37 observed in field-collected WSBA samples, suggesting that the aqueous-phase  
38 reactions might contribute to the formation of emitted biomass burning aerosols. The  
39 aqueous photochemistry of both the phenols (photooxidation) and WSBA extracts  
40 (direct photolysis) could produce a series of highly oxygenated compounds which in  
41 turn increases the oxidation degree of organic composition and acidity of the bulk  
42 solution. In particular, the LC/ESI-HRMS technique revealed significant  
43 photochemical evolution of the WSOC composition in WSBA samples, e.g., the  
44 photodegradation of low oxygenated species and the formation of highly oxygenated  
45 products. We also tentatively compared the mass spectra of photolytic time-profile  
46 WSBA extracts with each other for a more comprehensive description of the photolytic

47 evolution. The calculated average oxygen-to-carbon ratio (O/C) of oxygenated  
48 compounds in bulk extract increases from  $0.38 \pm 0.02$  to  $0.44 \pm 0.02$  (mean  $\pm$  standard  
49 deviation) while the intensity (S/N)-weighted average O/C ( $O/C_w$ ) increases from  $0.45$   
50  $\pm 0.03$  to  $0.53 \pm 0.06$  as the time of irradiation extends from 0 to 12h. These findings  
51 indicate that the water soluble organic fraction of combustion-derived aerosols has the  
52 potential to form more oxidized organic matter, contributing to the highly oxygenated  
53 nature of atmospheric organic aerosols.

## 54 **1 INTRODUCTION**

55 Water-soluble organic carbon (WSOC) comprises a significant fraction of  
56 atmospheric aerosols, accounting for 20–80% of total organic carbon (OC) (Krivacsy  
57 et al., 2001; Wozniak et al., 2008; Fu et al., 2015; Xie et al., 2016). WSOC is directly  
58 involved in the formation of cloud condensation nuclei (CCN) by modifying the  
59 aqueous chemistry and surface tension of cloud droplets (Graham et al., 2002; Nguyen  
60 et al., 2012; Zhao et al., 2013; McNeill 2015). Despite its significance, little is known  
61 about the chemical composition and sources of WSOC, with less than 10–20% of the  
62 organic mass being structurally identified (Cappiello et al., 2003; Fu et al., 2015).  
63 Biomass burning is a well-known emission source of WSOC (Anastasio et al., 1997;  
64 Fine et al., 2001; Graham et al., 2002; Mayol-Bracero et al., 2002; Gilardoni et al.,  
65 2016). Although the composition varies with fuel type and combustion conditions  
66 (Simoneit 2002; Smith et al., 2009), the WSOC mixture often covers a common range  
67 of polar and oxygenated aromatic compounds (Graham et al., 2002; Mayol-Bracero et  
68 al., 2002; Duarte et al., 2007; Chang and Thompson 2010; Yee et al., 2013; Gilardoni

69 et al., 2016) with molecules incorporating different numbers of functional groups like  
70 hydroxyl, carboxyl, aldehyde, ketone, ester, amino and/or other nitrogen-containing  
71 groups (Graham et al., 2002). In particular, lignin pyrolysis often yields a large amount  
72 of aromatic alcohols, carbonyls, and acid compounds (Mayol-Bracero et al., 2002;  
73 Chang and Thompson 2010; Gilardoni et al., 2016). Once dissolved into cloud, fog, and  
74 even aerosol liquid water, these substances can undergo aqueous-phase reactions to  
75 generate low-volatility species under sunlight irradiation, which have the potential to  
76 form secondary organic aerosol (SOA) after water evaporation (Graham et al., 2002;  
77 Cappiello et al., 2003; Duarte et al., 2007; Sun et al., 2010; Yu et al., 2014).

78 Field and laboratory studies have demonstrated that aqueous photochemical  
79 processes contribute significantly to the aqueous SOA formation from biomass burning  
80 precursors and the evolution of smoke particles (Sun et al., 2010; Lee et al., 2011;  
81 Kitanovski et al., 2014; Yu et al., 2014; McNeill 2015; Gilardoni et al., 2016). Gilardoni  
82 et al. (2016) observed aqueous SOA formation in both fog water and wet aerosols,  
83 resulting in an enhancement in the oxidized OA, and following atmospheric aging the  
84 overall oxidation degree of aerosols has also increased. In laboratory studies, phenols  
85 and methoxyphenols (important biomass burning intermediates) are often used as SOA  
86 precursors to examine the photochemical evolution in aqueous environments and  
87 aerosol-forming potential under relevant atmospheric conditions (Chang and  
88 Thompson 2010; Sun et al., 2010; Smith et al., 2014; Yu et al., 2014; Vione et al., 2019).  
89 The corresponding photochemical products formed through hydroxylation,  
90 oligomerization, and fragmentation typically cover a series of low-volatility and highly

91 oxygenated species. For instance, the methoxyphenol-derived SOA are proposed as a  
92 proxy for atmospheric humic-like substances (HULIS) (Ofner et al., 2011; Yee et al.,  
93 2013). Other compounds emitted from lignin pyrolysis, e.g., aromatic alcohol, carbonyl,  
94 and carboxylic species retaining the phenyl ring have also been found to produce  
95 colored products via aqueous photooxidation, which may become a part of HULIS  
96 (Chang and Thompson 2010; Huang et al., 2018). In addition, photochemical  
97 processing of common water-soluble aliphatic compounds such as aldehydes (Lim and  
98 Turpin 2015), polyols (Daumit et al., 2014), and organic acids (Griffith et al., 2013) in  
99 aqueous solution can also lead to the formation of oligomers, highly oxygenated and  
100 multifunctional organic matter (McNeill 2015).

101 In recent years, high resolution mass spectrometry (HRMS) has been commonly  
102 applied to study the organic molecular composition in cloudwater (Zhao et al., 2013;  
103 Boone et al., 2015), fogwater (Cappiello et al., 2003), rainwater (Altieri et al., 2009a;  
104 Altieri et al., 2009b), laboratory-generated SOA (Bateman et al., 2011; Romonosky et  
105 al., 2015; Lavi et al., 2017), and field-collected aerosol samples (Laskin et al., 2009;  
106 Lin et al., 2012a; Lin et al., 2012b; Kourtchev et al., 2013; Tong et al., 2016; Wang et  
107 al., 2017). It has also been used in time-profile observations of the photochemical  
108 evolution of aqueous extracts from laboratory-generated SOAs (Bateman et al., 2011;  
109 Romonosky et al., 2015). However, direct infusion MS methods are prone to ion  
110 suppression caused by other organic species, inorganic salts, and adduct formation  
111 (Kourtchev et al., 2013). Therefore, HRMS coupled with liquid chromatography (LC)  
112 might be another complementary powerful tool for relieving ion suppression due to its

113 abilities to separate and analyze different kind of compounds with differences in LC  
114 retention time (Kourtchev et al., 2013; Wang et al., 2016). It could also provide more  
115 information enabling the identification of possible isomers from the ions with same  
116 mass-to-charge ratio (m/z).

117 To our knowledge, the aqueous photochemical evolution of WSOC extracted from  
118 real ambient aerosols has not been studied in detail at the molecular level. Our previous  
119 study has revealed that the ultraviolet-visible (UV-VIS) absorption spectra of aqueous  
120 extracts from field biomass burning aerosols were modified under simulated sunlight  
121 illumination (Cai et al., 2018). Based on the previously studied field-collected samples,  
122 the present study is focused on a further analysis to investigate the molecular  
123 characteristics of water-soluble organic molecules by the photochemical evolution  
124 using electrospray ionization (ESI)-HRMS and LC/ESI-HRMS performed in negative  
125 ionization mode. For comparison, we also evaluated the photochemistry of phenol and  
126 guaiacol (representing the basic structures of phenols emitted from lignin pyrolysis)  
127 under laboratory conditions, and tentatively traced some of their photochemical  
128 products (e.g. dimers) in field-collected samples under study.

## 129 **2 EXPERIMENTAL SECTION**

### 130 **2.1 Particulate sample collection and preparation of aqueous extracts**

131 The wheat straw burning aerosol (WSBA) samples were collected during the summer  
132 harvest season of 2013, at rural fields in the plain of north China where the wheat was  
133 the main agricultural crop (Cai et al., 2018). To facilitate subsequent planting and

134 management, a large amount of fresh wheat straw was directly burned in the field during  
135 the harvest season, and the water emitted from burning plant body could provide a  
136 suitable environment for aqueous photochemistry of dissolved compounds. The  
137 selected WSBA samples used for HRMS analysis were collected from two sampling  
138 sites, located at rural fields in Wenxian in Henan Province (noted: HNWX) and Daming  
139 in Hebei Province (HBDM). As described in Cai et al. (2018), the selected sampling  
140 sites were mainly affected by heavy smog from wheat straw burning (Figure 1). The  
141 emitted fine particulate matter with aerodynamic diameter  $\leq 2.5\mu\text{m}$  ( $\text{PM}_{2.5}$ ) was  
142 collected at a flow rate of  $5\text{ L min}^{-1}$  by a portable particulate sampler (MiniVol TAS,  
143 AirMetrics, USA), with quartz fiber filters (47mm in diameter, QMA, Whatman, UK)  
144 baked at  $600^{\circ}\text{C}$  for 6 hours before sampling. The sampling flow rate was calibrated  
145 with a standard flow meter (Bios Defender 520) and the sampling time of each filter  
146 was restricted to 30-60 minutes depending on the ambient biomass burning aerosol  
147 concentration and expected filter loading (Cai et al., 2018). After collection, the filter  
148 samples were stored in dark and transported to the laboratory, and then stored at  $-20^{\circ}\text{C}$   
149 under a light-proof condition.

150 The preparation of WSOC extracts and measurements for carbon content including  
151 organic carbon (OC), elemental carbon (EC) and WSOC were described in detail in Cai  
152 et al. (2018). Briefly, a part of each quartz fiber filters ( $1.6\text{-}3.2\text{cm}^2$ ) was placed into a  
153 brown vial and extracted with ultra-pure water (Milli-Q, Milipore) for two times; at  
154 each time 5 ml ultra-pure water with a 30min ultrasonic agitation was applied. The two-  
155 time extracts were combined and filtered through a PTFE syringe filter ( $0.2\mu\text{m}$  pore

156 size, Thermo Scientific), followed by a pH measurement with a pH meter (Mettler  
157 Toledo SevenEasy™ S20) that has been regularly calibrated at pH 4.00 and 6.86. Prior  
158 to analysis the extracts were stored at -20°C in the dark. To reduce the WSOC mass loss,  
159 the desalting treatment (e.g., solid phase extraction (SPE)) was not performed on these  
160 samples.



161  
162 **Figure 1. One field site at Daming, Hebei province, China, for sampling the aerosols affected**  
163 **by biomass burning.**

## 164 **2.2 Direct photolysis of WSOC extracts**

165 A 12-hour direct photolysis of WSOC extracts obtained from WSBA samples was  
166 performed in a photo-reactor (BL-GHX-V, Bilon Instruments Co. Ltd., China, see  
167 Figure S1) that was equipped with a solar simulator (Xe lamp, 1000W) placed into a  
168 double-deck quartz condenser (Cai et al., 2018). A cooling water (18°C) was circulating  
169 in the outer tube of the condenser to avoid heating of the samples. In the wavelength  
170 range of 310-400 nm relevant to the boundary layer of the atmosphere, the actinic flux



171 of the lamp is about 5 times stronger than the solar actinic flux, meaning that the spectral  
172 evolution via the 12-hour simulated solar irradiation might be equal with the effect  
173 caused by actual sunlight irradiation with a duration of at least 60 hours (Cai et al.,  
174 2018). Air-tight quartz tubes (1.5cm in diameter, 3ml solution per tube) loading extracts  
175 were equidistantly arranged around the lamp. Each extract was distributed into three  
176 tubes that corresponded to three different irradiation times, i.e. 0, 4, and 12 h, with no  
177 oxidants added externally throughout the whole photolytic process. At each irradiation  
178 time point (e.g., 0 and 4 h), the related tubes were wrapped with aluminum foil, and  
179 placed at the initial location until the end of 12-h photolysis (Cai et al., 2018).

180 As described in Cai et al. (2018), the water extraction resulted in a dilution of the  
181 collected organic compounds, however, the ratio of the water mass to PM<sub>2.5</sub> mass for  
182 extract samples (ranging from  $1.8 \times 10^3$  to  $3.4 \times 10^4$ ) was compatible with the ratio of  
183 water mass to WSOC content in cloud water (in a wide range from  $1.4 \times 10^2$  to  $1.6 \times 10^4$ )  
184 (Li et al., 2017), indicating that the present aqueous extracts are relevant to the  
185 atmospheric cloud water condition.

### 186 **2.3 Photooxidation of phenolic compounds under laboratory conditions**

187 Initial solutions of 0.1 mM phenol (C<sub>6</sub>H<sub>6</sub>O) and 0.1 mM guaiacol (C<sub>7</sub>H<sub>8</sub>O<sub>2</sub>) in  
188 combination with an OH radical precursor (0.1 mM H<sub>2</sub>O<sub>2</sub>) were prepared in ultra-pure  
189 water (Milli-Q, Milipore). The pH of the solution was adjusted to 5 with 0.1 M sulfuric  
190 acid (H<sub>2</sub>SO<sub>4</sub>), which is usually relevant to the acidity in fog and cloud waters (Collet et  
191 al., 1998; Fahey et al., 2005). The prepared solution and reference blank were irradiated  
192 by simulated sunlight irradiation with a duration of 4 hours. Hereby, we mainly focus

193 on acquiring the chemical characteristics of aqueous products of phenols, and  
194 tentatively identify some tracer compounds (e.g., phenolic dimers) whether they exist  
195 in present biomass burning particulate samples.

#### 196 **2.4 Sample analysis**

197 The direct infusion MS analysis was conducted using a Thermo Scientific Orbitrap  
198 Fusion Tribrid mass spectrometer equipped with quadrupole, orbitrap, and linear ion  
199 trap mass analyzers, with a heated ESI source. To assist in ionization and desolvation,  
200 the sample was diluted to a 1:1 mixture of acetonitrile and sample by volume. The full  
201 scan mass spectra were acquired in negative ionization mode, with a resolution of 120  
202 000 at  $m/z$  200 for the Orbitrap analyzer and a mass scan range of  $m/z$  50-750. Before  
203 determination, the Orbitrap analyzer was externally calibrated for mass accuracy using  
204 Thermo Scientific Pierce LTQ Velos ESI calibration solution. The direct infusion  
205 parameters were as follows: sample flow rate  $5\mu\text{l min}^{-1}$ ; capillary temperature  $300^\circ\text{C}$ ;  
206 S-lens RF 65%; spray voltage  $-3.5\text{kV}$ ; sheath gas, auxiliary gas, and sweep gas flows  
207 were 10, 3, and 0 arbitrary units, respectively. Data collecting was performed when the  
208 intensity of the total ion current (TIC) maintained constant with a relative standard  
209 deviation (RSD) under 5%. At least 100 data points (mass spectral scans) were collected  
210 for each test sample, and the each exported mass spectrum for analysis was derived  
211 from the average result of 100 spectrums.

212 The LC/ESI-HRMS analysis operated in negative ionization mode was performed  
213 using a U3000 system coupled with a T3 Atlantis C18 column ( $3\mu\text{m}$ ;  $2.1\times 150\text{mm}$ ;  
214 Waters, Milford, USA) and an Orbitrap Fusion MS. A  $10\mu\text{L}$  sample was injected, with

215 a flow rate of 0.2 ml min<sup>-1</sup> for the mobile phase, which consisted of H<sub>2</sub>O (A) and  
216 acetonitrile (B). The gradient applied was 0-5 min 3% B; 5-20 min from 3 to 95%  
217 (linear), and kept for 25 min at 95%; and 45-50 min from 95 to 3%, and held for 10 min  
218 at 3% (total run time 60 min).

## 219 **2.5 Data processing**

220 Mass spectral peaks with three times larger than the signal to noise ratio (S/N) were  
221 extracted from the raw files. Peaks in both sample and blank spectra were retained if  
222 their intensity in the former was five times larger than in the latter. A common molecular  
223 assignment based on the accurate mass was performed using Xcalibur software (V3.0  
224 Thermo Scientific) with the following constraints: <sup>12</sup>C≤50, <sup>13</sup>C≤1, <sup>1</sup>H≤100, <sup>16</sup>O≤50,  
225 <sup>14</sup>N≤4, <sup>32</sup>S≤1, and <sup>34</sup>S≤1. All mathematically possible elemental formulas, with a mass  
226 tolerance of ±3ppm were calculated. Elemental formulas containing <sup>13</sup>C or <sup>34</sup>S were  
227 checked for the presence of <sup>12</sup>C or <sup>32</sup>S counterparts, respectively. If they were not  
228 matched with the corresponding monoisotopic formulas, then the assignment with next  
229 larger mass error was considered. Isotopic and unassigned peaks were excluded from  
230 further analysis.

231 Ions were also characterized by the number of rings plus double bonds (i.e., double  
232 bond equivalents (DBE)), which were calculated as:  $DBE = c - h/2 + n/2 + 1$  for an  
233 elemental composition of C<sub>c</sub>H<sub>h</sub>O<sub>o</sub>N<sub>n</sub>S<sub>s</sub>. The assigned formula was additionally checked  
234 with the nitrogen rule. For ambient samples, based on the presence of various elements  
235 in a molecule, the identified elemental formulas were classified into several main  
236 compound classes: CHO (i.e., molecules containing only C, H, and O atoms), CHOS,

237 CHON, and CHONS, and others including CHN and CHS. In the present study, because  
238 the detected water-soluble ions almost were below  $m/z$  400, we focused our molecular  
239 analysis on  $m/z$  50-400.

## 240 **3 RESULTS AND DISCUSSION**

### 241 **3.1 Mass spectral characteristics of WSOC extracts from WSBA samples**

242 The preliminary analysis showed that the  $PM_{2.5}$  concentration in ambient air near to  
243 the burning sites ranged from 6.46 to 28.03  $mg\ m^{-3}$  (Table S1). OC was the major  
244 component of the collected  $PM_{2.5}$  with a proportion of  $50.9 \pm 7.6\%$  (mean  $\pm$  standard  
245 deviation), whereas EC represented a negligible fraction (average  $1.3 \pm 0.4\%$ ).  
246 Meanwhile, WSOC accounted for  $35.5 \pm 7.5\%$  of OC in the tested samples.

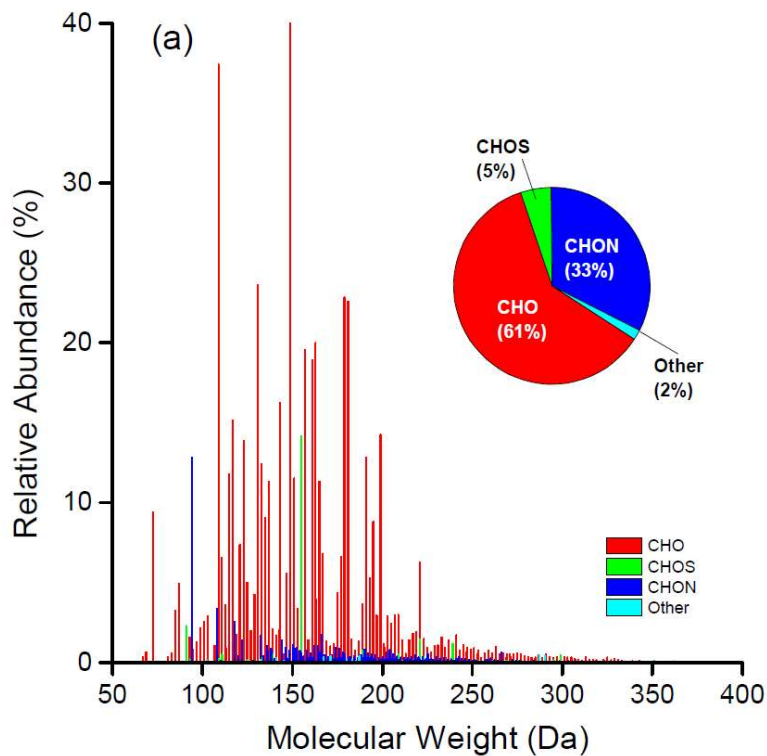
247 Although this batch of aerosol samples were collected from different sites, their  
248 water-extracted solutions showed similar light-absorbing characteristics in UV-VIS  
249 absorption spectra (Cai et al., 2018). Here, four extract samples (HNWX-1, HNWX-2,  
250 HBDM-1 and HBDM-2) (Table S1) were chosen for further analysis using high  
251 resolution mass spectrometry. These samples also exhibited similar patterns in mass  
252 distribution of water-soluble molecular species that mainly range from 50 to 400 Da,  
253 which indicated a similar burning source for these samples. A reconstructed mass  
254 spectrum (subtracted blank) for one representative sample of HNWX-1 is shown in  
255 Figure 2a (others are shown in Figure S2). In mass range 50-400 Da, there were  $827 \pm$   
256 44 molecular formulas identified throughout the all samples, and most of the formulas  
257 (above 75%) were overlapped between these analyzed samples. The classification  
258 features of assigned compounds for analyzed extracts are shown in Table S2. In the

259 amount of assigned formulas, CHO composition was the most abundant group,  
260 accounting for  $59.2 \pm 2.2\%$  of the total assignments, followed by CHON ( $35.0 \pm 2.2\%$ ).  
261 These results are consistent with previous observations of laboratory-generated biomass  
262 burning aerosol (Smith et al., 2009) and field particulate samples influenced by biomass  
263 combustion (Kourtchev et al., 2016) in spite of the differences of biomass varieties,  
264 extracted solvents, and HRMS techniques between present and previous studies.

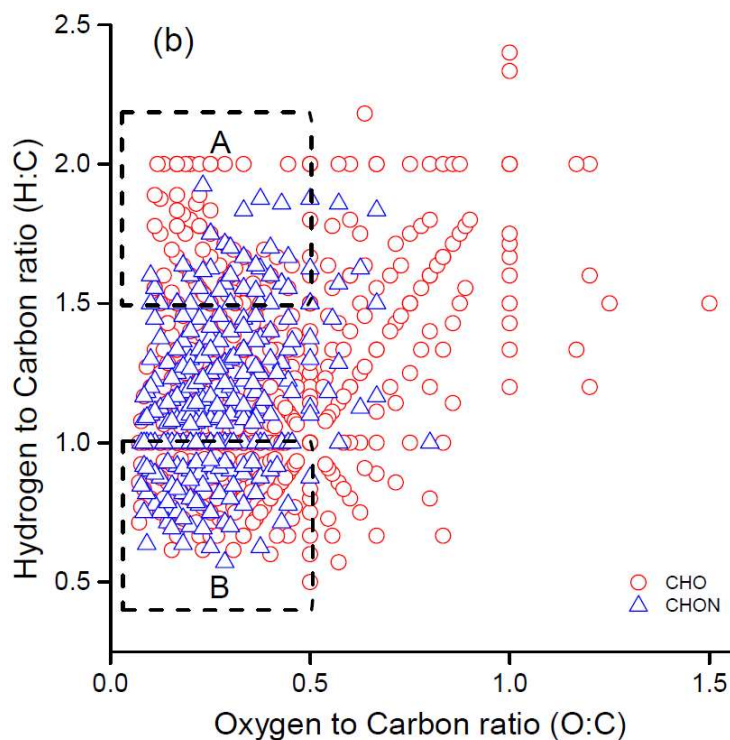
265 On the other hand, CHOS and CHONS compounds contributed with less than 5% to  
266 the total assignment. A number of studies have shown the wide presence of  
267 organosulfates and nitrooxy-organosulfates in urban (Lin et al., 2012b; Wang et al.,  
268 2016), rural (Lin et al., 2012a), and forest aerosols (Kourtchev et al., 2013), and even  
269 in cloudwater (Boone et al., 2015); however, most of these compounds were not  
270 observed in our negative mass spectra. This could be accounted for by the low extent  
271 of aerosol evolution, due to the limited oxidation conditions available for the formation  
272 of organosulfates and nitrooxy-organosulfates in fresh smoke aerosols. For example,  
273 laboratory studies have observed the significant formation of organosulfates via  
274 photooxidation in the presence of acidic sulfate aerosol (with significant level of SO<sub>2</sub>  
275 concentration) (Surratt et al., 2007; Surratt et al., 2008). All detected ion species with  
276 enabled formula assignments in present samples are listed in Table S3. The electrospray  
277 ionization did not ionize well CHN and CHS compounds; hence, they were not the most  
278 prevalent compounds in present samples.

279 It should be also noted that the negative ionization mode prefers to detect those  
280 molecules containing polar functional groups (e.g., -OH and -COOH) that could be

281 readily deprotonated. There were number of compounds that were not easily  
282 deprotonated and might show up preferentially in positive ionization mode (e.g.  
283 amines). Furthermore, the formula numbers detected in the HRMS potentially contain  
284 multiple structural isomers; therefore, the actual number of water-soluble organic  
285 species is expected to be underestimated. The additional LC/ESI-HRMS analysis  
286 operated in negative mode confirmed a substantial number of ion masses (e.g., assigned  
287 CHO and CHON compounds) containing more than one structural isomer, which could  
288 be observed at different retention times (RTs) in chromatograms. Two representative  
289 groups of extracted chromatograms for CHO ( $[C_7H_5O_n]^-$ , (n=2~4)) and CHON  
290 ( $[C_7H_5O_nN]^-$ , (n=1~3)) compounds are shown in Figure S3 and S4, respectively, where  
291 increasing the O or N atom number in a molecule might lead to more isomer peaks.  
292 However, it should be noted that these LC-separated peaks might also include other  
293 unidentified compounds that were outside of the elemental assignment considered in  
294 this study. Additionally, low mass loading and potential decomposition under the  
295 ionization can also limit the detection of some high molecular weight species.



296



297

298 **Figure 2. (a) Reconstructed mass spectra for detected ions with assigned formulas and (b)**  
 299 **Van Krevelen diagrams for CHO and CHON species in extract of HNWX-1 sample. The**  
 300 **inset pie charts in (a) show the number fraction of each class in the total assigned**  
 301 **compounds. Areas A and B in (b) are tentatively attributed to aliphatic and aromatic species,**  
 302 **respectively.**

303 The interpretation of the complex organic mass spectra generated by high resolution  
304 mass spectrometry can be simplified by plotting the hydrogen to carbon ratio (H/C)  
305 against the oxygen to carbon ratio (O/C) for individual assigned atomic formulas in  
306 form of the Van Krevelen (VK) diagram (e.g. Lin et al., 2012a; Kourtchev et al., 2013).  
307 Figure 2b indicates a representative VK diagram of CHO and CHON compounds  
308 derived from HNWX-1 sample. It can be clearly seen from Figure 2b that the majority  
309 of CHO and CHON molecules are located at the region of  $O/C \leq 1.0$  and  $H/C \leq 2.0$ . In  
310 VK diagram, molecules with  $H/C \leq 1.0$  and  $O/C \leq 0.5$  are typical for aromatic species,  
311 while molecules with  $H/C \geq 1.5$  and  $O/C \leq 0.5$  would be associated with typical  
312 aliphatic compounds (Mazzoleni et al., 2012; Kourtchev et al., 2014). The average  
313 double bond equivalent (DBE) showed relative high values with 5.5 for CHO  
314 compounds and 6.1 for CHON compounds (Table S2), suggesting that oxidized  
315 aromatic compounds were abundant in the present sample, and their presence could  
316 partially account for the strong light-absorbing feature in the near-UV region as  
317 observed in our previous study (Cai et al., 2018).

318 The average H/C and O/C values throughout the extract samples were in the ranges  
319 of 1.26-1.31 and 0.34-0.42 for CHO compounds, 1.19-1.23 and 0.28-0.29 for CHON  
320 compounds (shown in Table S2), respectively. Although the ESI analysis were  
321 performed in the negative ionization mode, the measured O/C exhibit rather low values,  
322 which fall in the range of O/C ratios typical for biomass burning organic aerosol derived  
323 from positive ionization mode (Aiken et al., 2008; Kourtchev et al., 2016). Due to fresh  
324 emission and smaller aging effect, the present O/C were obviously lower than the O/C



325 of long-range transport biomass burning aerosols (Zhang et al., 2018).

326 Carbon oxidation state ( $OS_c$ ) was observed to increase with oxidation for  
327 atmospheric organic aerosol and link strongly to aerosol volatility (Kroll et al., 2011).

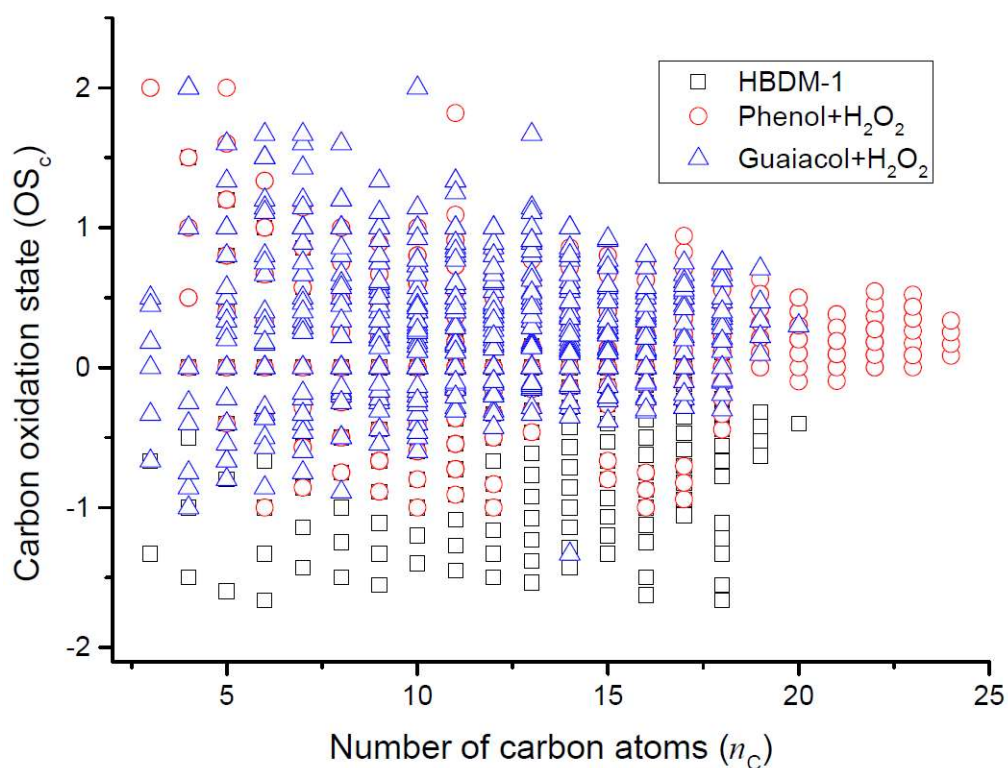
328  $OS_c$  for each molecular formula can be calculated using the following equation:

329 
$$OS_c = - \sum_i OS_i \frac{n_i}{n_c}$$

330 where  $OS_i$  is the oxidation state associated with non-carbon element  $i$  and  $n_i/n_c$  is the

331 molar ratio of element  $i$  to carbon within the molecule (Kroll et al., 2011; Kourtchev et

332 al., 2013).



333

334 **Figure 3. The distribution of carbon oxidation state ( $OS_c$ ) for CHO molecules in HBDM-1**  
335 **and laboratory samples.**

336 Considering that nitrogen and sulfur atoms can present multiple oxidation states, the

337  $OS_c$  was calculated and analyzed only for CHO compounds in this study. A similar

338 pattern of OSc values versus the number of carbon atoms ( $n_C$ ) was observed for CHO  
339 compounds detected in present WSBA samples (Figure 3 and Figure S5). From Figure  
340 3 and Figure S5, it can be seen that OSc of each sample ranges mainly from -1.5 to +1  
341 with average ranging from -0.6 to -0.4. Consistent with previous studies (Kroll et al.,  
342 2011; Kourtchev et al., 2016), the majority of molecules with  $OS_C < 0$  (low oxidized  
343 organics) and carbon atoms lower than 20 are suggested to be associated with the  
344 primary organic aerosols emitted from biomass burning. A minor fraction of molecular  
345 formulas with  $OS_C \geq 0$  values might be associated with semivolatile and low-volatility  
346 oxidized organic aerosols (Kroll et al., 2011). Figure 3 also shows the plot of  $OS_C$  versus  
347  $n_C$  for products obtained from photooxidation of phenol and guaiacol, respectively, and  
348 their comparison with WSBA samples will be discussed in section 3.3.

### 349 **3.2 Mass spectral characteristics of the products from photooxidation of phenolic** 350 **compounds in the aqueous phase**

351 Phenol and guaiacol were chosen as two representative model compounds derived  
352 from biomass combustion. Two high resolution mass spectra of aqueous phenol and  
353 guaiacol exposed to OH radicals for 4h are shown in Figure S6, where 435  $C_xH_yO_z$   
354 molecular formulas ( $m/z$  90-500) were assigned for product ions of phenol (with  $C_3$ -  
355  $C_{24}$ ) and 624  $C_xH_yO_z$  formulas ( $m/z$  90-600) were assigned for product ions of guaiacol  
356 (with  $C_3$ - $C_{27}$ ). The average H/C and O/C values were  $0.79 \pm 0.28$  and  $0.52 \pm 0.23$  for  
357 phenol, and  $0.88 \pm 0.24$  and  $0.59 \pm 0.24$  for guaiacol, respectively. Clearly, the  
358 photochemical processing induced by OH oxidation resulted in an increase in average  
359 O/C of product molecules relative to their precursors (O/C=0.17 for phenol and O/C=

360 0.29 for guaiacol).

361 The formation mechanisms of series of oxygenated products, e.g., phenolic  
362 oligomers, hydroxylated phenolic species, ring-opening and highly oxygenated  
363 compounds, are proposed in the literature (e.g. Sun et al., 2010; Chang and Thompson,  
364 2010; Yu et al., 2014; Huang et al., 2018). The OH-initiated reactions would result in  
365 enhanced hydroxylation of the aromatic ring as well as in increased yields of carboxylic  
366 acids and toxic dicarbonyl compounds (Sun et al., 2010; Yu et al., 2014; Prasse et al.,  
367 2018). For example, some highly oxygenated C<sub>2</sub>-C<sub>5</sub> aliphatic compounds (e.g., C<sub>2</sub>H<sub>2</sub>O<sub>4</sub>,  
368 C<sub>3</sub>H<sub>4</sub>O<sub>4</sub>, C<sub>4</sub>H<sub>6</sub>O<sub>4</sub>, and C<sub>5</sub>H<sub>6</sub>O<sub>5</sub>) corresponding to carboxylic acids (Yu et al., 2014) were  
369 clearly observed in the mass spectra of present photochemical products. The occurrence  
370 of these oxygenated products not only directly increased the degree of oxygenation in  
371 the bulk solution composition, but also contributed to the variation of solution acidity.  
372 After the 4-hours photochemical process, the pH values of the irradiated solution were  
373 significantly lower than the pH values of the solution prior to irradiation (t-test,  $p < 0.05$ ),  
374 and the calculated acidities ( $[H^+]$ ) of the bulk solution increased by  $(2.96 \pm 0.15) \times 10^{-5}$   
375 M and  $(4.26 \pm 0.16) \times 10^{-5}$  M for phenol and guaiacol, respectively.

376 The oligomerization induced by photochemical transformation of phenolic  
377 substances is an important formation pathway for low-volatility, light-absorbing  
378 compounds (Smith et al., 2016). Here, phenolic dimers (i.e., C<sub>12</sub>H<sub>10</sub>O<sub>2</sub> for phenol  
379 dimer and C<sub>14</sub>H<sub>14</sub>O<sub>4</sub> for guaiacol dimer) and higher oligomers (e.g., C<sub>18</sub>H<sub>14</sub>O<sub>3</sub> and  
380 C<sub>24</sub>H<sub>18</sub>O<sub>4</sub> for phenol trimer and tetramer, C<sub>21</sub>H<sub>20</sub>O<sub>6</sub> for guaiacol trimer), as well as their  
381 hydroxylated species were observed. The formation mechanism can be ascribed to C-

382 O or C-C coupling of phenoxy radicals that were formed via H-abstraction of the  
383 phenols or OH addition to the aromatic ring (Net et al., 2009, Sun et al, 2010). The  
384 reaction at the para position or para-para coupling was more likely to occur due to a  
385 higher probability of free electron to occur in this position (Lavi et al, 2017) or a weaker  
386 steric hindrance in the para position.

### 387 **3.3 Comparison of the photochemical products of phenolic compounds and the** 388 **CHO composition in WSOC extracts from WSBA samples**

389 Compared to the CHO compounds detected in WSOC extracts, the photochemical  
390 products of the two phenols under study showed a higher O/C and a lower H/C values.  
391 The average  $OS_C$  of photochemical products from phenol ( $OS_C=-0.7$ ) and guaiacol  
392 ( $OS_C=-0.6$ ) after a 4-hour photooxidation raised to +0.2 and +0.3, respectively, showing  
393 distinctly a higher degree of oxidation than the present WSBA samples. In Figure 3,  
394 more species with  $OS_C < 0$  (especially  $OS_C < -0.5$ ) are presented in the field sample  
395 (HBDM-1), while the species with  $OS_C \geq 0$  are prevalent in photochemical products of  
396 phenol and guaiacol. The single-precursor systems in laboratory did not completely  
397 reflect the CHO composition features in water-soluble extracts from real straw-burning  
398 samples that contained a myriad of precursors and unknown substances from  
399 atmospheric background, soil and other sources. Considering that a large number of  
400 phenols and methoxyphenols exist in the straw-burning smokes and their potential to  
401 undergo photochemical aging, the nature of emitted primary organic aerosols is  
402 reasonably more complicated than the nature of simulated products derived from single-  
403 precursor systems.

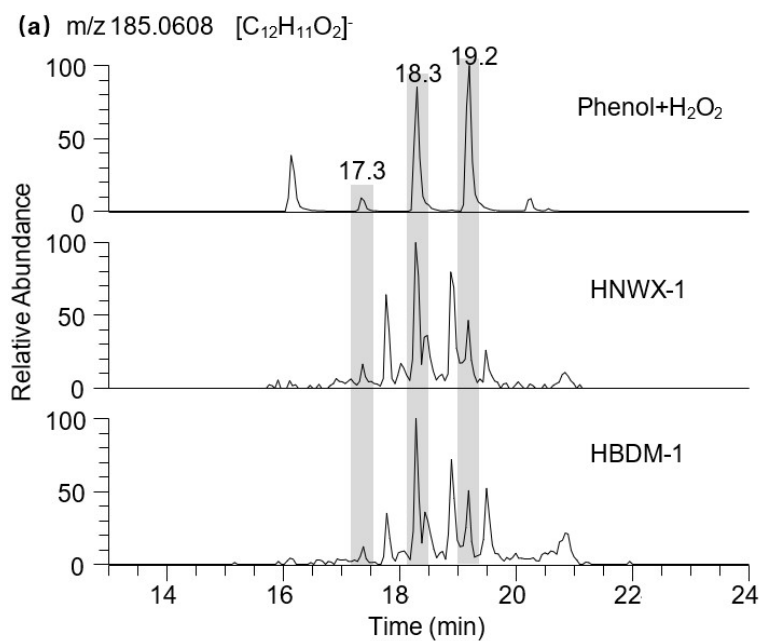
404 The extracted LC chromatograms of  $m/z$  185.0608 and 245.0823 are shown in Figure  
405 4, respectively, where both ions involve dimers of phenol and guaiacol with several  
406 structures, and/or other isomers. The presence of guaiacol dimer and syringol dimer  
407 was previously observed in aerosol samples largely affected by wood combustion.  
408 Based on the Aerosol Mass Spectrometer (AMS) analysis, these two dimers were  
409 suggested as markers of biomass burning aerosols (Sun et al., 2010; Yu et al., 2014). In  
410 the composition of present biomass burning aerosols, the phenolic dimers ( $m/z$   
411 185.0608 and 245.0823) were also observed in present mass spectra, but the extracted  
412 LC chromatograms shown in Figure 4 indicate that these ions contain multiple RT peaks.  
413 The same peaks with RT 18.3 and 19.2 min which are assumed to be the phenol dimers  
414 were observed during the photochemical transformation of phenol (Figure 4a) and in  
415 the WSBA samples. Meanwhile, the present particle extracts may also involve guaiacol  
416 dimer, since its  $m/z$  245.0823 has two LC peaks emerged at RT 17.7 and 19.5 min  
417 (Figure 4b) same as the peaks identified during the photochemical transformation of  
418 guaiacol. Considering a large amount of water emitted during the process of straw  
419 combustion, the occurrence of phenolic dimers might indicate that the aqueous phase  
420 reactions played an important role in the formation and evolution of emitted aerosol  
421 organic composition.

422 Typical hydroxylated species such as, e.g.,  $C_2H_2O_4$ ,  $C_6H_6O_2$ ,  $C_7H_6O_3$ ,  $C_7H_8O_3$ , were  
423 also found in the samples from photooxidation of both phenols and the WSBA samples.  
424 The comparison of the photochemical products from phenols and the WSBA samples  
425 revealed their significant difference, pointing to the importance of studying real aerosol

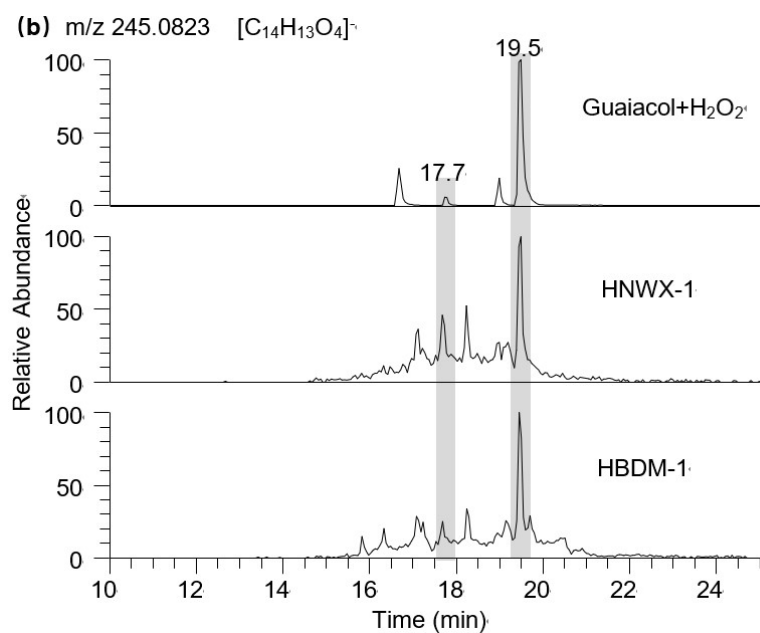
426 samples against the laboratory model compounds. However, evaluating the model  
427 compounds as proxy of real aerosol samples is always helpful as a reference. To this  
428 end, it is worth noting that potentially other phenols and methoxyphenols (e.g.,  
429 acetosyringone, vanillin) that dissolve into cloud, fog droplets or aerosol liquid water  
430 can be photochemically transformed and contribute to the SOA formation (Vione et al.,  
431 2019, Zhou et al., 2019).

### 432 **3.4 Photolysis of WSOC extracts from WSBA samples**

433 Although the direct photolysis was performed on present WSOC extracts from WSBA  
434 samples in presence of simulated sunlight irradiation without adding any oxidants, the  
435 photooxidation process still occurred since the particle extracts were very likely to  
436 include various oxidants, e.g., singlet molecular oxygen ( $^1\text{O}_2$ ), peroxides, hydroxyl  
437 radical (OH) or excited triplet state of organics produced under light excitation  
438 (Anastasio et al., 1997; Vione et al., 2006; Net et al., 2009; Net et al., 2010a; Bateman  
439 et al., 2011; Rossignol et al., 2014; Smith et al., 2014; Gómez Alvarez et al., 2012). In  
440 particular, the excited triplet state of aromatic carbonyls (e.g., 3, 4-  
441 dimethoxybenzaldehyde) (Net et al., 2010b) was found to be more efficient than OH  
442 radical to oxidize phenols and produce hydroxylated species (Smith et al., 2014., Yu et  
443 al., 2014). This photosensitized reaction is likely to play an important role in the WSOC  
444 evolution, due to high quantities of aromatic carbonyls present in the extracts of  
445 biomass burning aerosols.



446



447

448 **Figure 4. Extracted LC chromatograms of (a)  $m/z$  185.0608 and (b)  $m/z$  245.0823 in**  
 449 **photochemical sample of phenol, HNWX-1, and HBDM-1, respectively.**

450 The variation in peak abundance at unique retention times in the chromatogram could  
 451 reflect the extent of evolution of WSOC molecules with accurate molecular weights,  
 452 although no available standards were utilized for absolute quantification. The LC/ESI-  
 453 HRMS monitors obviously changes in the molecular features of partial CHO species,

454 i.e., photodegradation of low oxygenated compounds and formation of high oxygenated  
455 compounds. Table 1 lists the CHO compounds for which the LC peak intensities  
456 significantly increased and decreased after the 12-hour photolysis.

### 457 **3.4.1 Photodegradation of low oxygenated compounds and formation of highly** 458 **oxygenated compounds**

459 As shown in Table 1, ion masses assigned with high unsaturated and low oxygenated  
460 species ( $O/C < 0.5$ ) are prone to photodegradation, especially  $C_7$ - $C_9$  compounds  
461 (possible aromatic species), which intensity decreased by nearly one order of magnitude.  
462 For example, for  $m/z$  123.0450 ( $[C_7H_7O_2]^-$ ), as shown in Figure 5a, the peaks at RT 16.2  
463 and 16.7 min in the LC chromatogram reduced in area by 95% after the 12-h irradiation.  
464 Using a standard it was verified that both peaks did not belong to guaiacol (peak at  
465 RT17.3 min), but they were also found within the products of guaiacol photooxidation,  
466 suggesting that they might be isomers of guaiacol or aromatic dihydric alcohol.

467 The phenolic dimers ( $C_{12}H_{10}O_2$  and  $C_{14}H_{14}O_4$ ) as described above also exhibited a  
468 decreasing tendency with almost complete disappearance after 12h direct photolysis.  
469 Other species with relatively high MW ( $\geq 200Da$ ) were also observed to be  
470 decomposed, including  $m/z$  251.0564 ( $[C_{12}H_{11}O_6]^-$ ), 313.0724 ( $[C_{17}H_{13}O_6]^-$ ), and  
471 329.0674 ( $[C_{17}H_{13}O_7]^-$ ) (Figure S7), although their initial abundance was not very high.

472 On the other hand, the solution acidity ( $[H^+]$ ) of the particle extracts increase after  
473 the 12-hour photolysis, similar to the observation on the photooxidation of phenols  
474 (section 3.2) that resulted in the formation of oxygenated species. The solution acidity  
475 ( $[H^+]$ ) normalized by WSOC concentration ( $[OC_{ws}]$ ) was increased with a variation of



476  $\Delta[\text{H}^+]/[\text{OC}_{\text{ws}}]=(3.8 \pm 0.8) \times 10^{-7}$  mol mgC<sup>-1</sup>, suggesting the formation of new acidic  
 477 substances.

478 **Table 1. *M/Z* with significant changes upon 12-h photolysis analyzed by LC/ESI-HRMS.**

Precursor (LC peak intensity decreases by >50%)			Product (LC peak intensity increases by >50%)		
Retention time, min	Measured <i>m/z</i>	Molecular formula	Retention time, min	Measured <i>m/z</i>	Molecular formula
16.2,16.7	123.04497	C <sub>7</sub> H <sub>8</sub> O <sub>2</sub>	1.9	59.01362	C <sub>2</sub> H <sub>4</sub> O <sub>2</sub>
13.9,14.5	129.05555	C <sub>6</sub> H <sub>10</sub> O <sub>3</sub>	1.8	72.99291	C <sub>2</sub> H <sub>2</sub> O <sub>3</sub>
14.6	131.07121	C <sub>6</sub> H <sub>12</sub> O <sub>3</sub>	2.1	73.02928	C <sub>3</sub> H <sub>6</sub> O <sub>2</sub>
14.6	133.02934	C <sub>8</sub> H <sub>6</sub> O <sub>2</sub>	1.8	75.00856	C <sub>2</sub> H <sub>4</sub> O <sub>3</sub>
15.9	135.04498	C <sub>8</sub> H <sub>8</sub> O <sub>2</sub>	2.4	85.02930	C <sub>4</sub> H <sub>6</sub> O <sub>2</sub>
13.7	137.02426	C <sub>7</sub> H <sub>6</sub> O <sub>3</sub>	1.9, 4.4	87.04496	C <sub>4</sub> H <sub>8</sub> O <sub>2</sub>
17.7	137.06063	C <sub>8</sub> H <sub>10</sub> O <sub>2</sub>	1.9	88.98785	C <sub>2</sub> H <sub>2</sub> O <sub>4</sub>
15.8	147.04504	C <sub>9</sub> H <sub>8</sub> O <sub>2</sub>	1.9	89.02427	C <sub>3</sub> H <sub>6</sub> O <sub>3</sub>
17.2	149.06062	C <sub>9</sub> H <sub>10</sub> O <sub>2</sub>	2.2	99.00857	C <sub>4</sub> H <sub>4</sub> O <sub>3</sub>
19.0	151.07634	C <sub>9</sub> H <sub>12</sub> O <sub>2</sub>	2.5	129.01917	C <sub>5</sub> H <sub>6</sub> O <sub>4</sub>
16.8	161.06068	C <sub>10</sub> H <sub>10</sub> O <sub>2</sub>	2.0	145.01407	C <sub>5</sub> H <sub>6</sub> O <sub>5</sub>
16.2	165.05559	C <sub>9</sub> H <sub>10</sub> O <sub>3</sub>	1.9	147.02971	C <sub>5</sub> H <sub>8</sub> O <sub>5</sub>
14.9	167.07129	C <sub>9</sub> H <sub>12</sub> O <sub>3</sub>	14.9	155.03482	C <sub>7</sub> H <sub>8</sub> O <sub>4</sub>
15.1	181.05048	C <sub>9</sub> H <sub>10</sub> O <sub>4</sub>	15.1	169.01411	C <sub>7</sub> H <sub>6</sub> O <sub>5</sub>
17.3	191.03498	C <sub>10</sub> H <sub>8</sub> O <sub>4</sub>	16.4	183.02980	C <sub>8</sub> H <sub>8</sub> O <sub>5</sub>
16.2	195.06622	C <sub>10</sub> H <sub>12</sub> O <sub>4</sub>			
18.6	207.06635	C <sub>11</sub> H <sub>12</sub> O <sub>4</sub>			

479 The photochemical processing has led to an increased formation of low MW  
 480 compounds (e.g., C<sub>2</sub>-C<sub>5</sub> species), with a relatively high O/C. For example, the C<sub>2</sub>  
 481 compounds, including [C<sub>2</sub>H<sub>1</sub>O<sub>3</sub>]<sup>-</sup>, [C<sub>2</sub>H<sub>3</sub>O<sub>3</sub>]<sup>-</sup>, [C<sub>2</sub>H<sub>3</sub>O<sub>2</sub>]<sup>-</sup>, and [C<sub>2</sub>H<sub>1</sub>O<sub>4</sub>]<sup>-</sup> (Figure S8),  
 482 which may correspond to glyoxylic acid, glycolic acid, acetic acid, and oxalic acid,  
 483 respectively, were likely to be formed via oxidation pathway of several water-soluble  
 484 molecules with photochemical reactivity (e.g., glyoxal (Carlton et al., 2007; Lim et al.,  
 485 2010), methylglyoxal (Altieri et al., 2008; Lim et al., 2010), pyruvic acid (e.g. Grgic et  
 486 al., 2010; Griffith et al., 2013; Reed Harris et al., 2014; Rapf et al., 2017; Eugene and

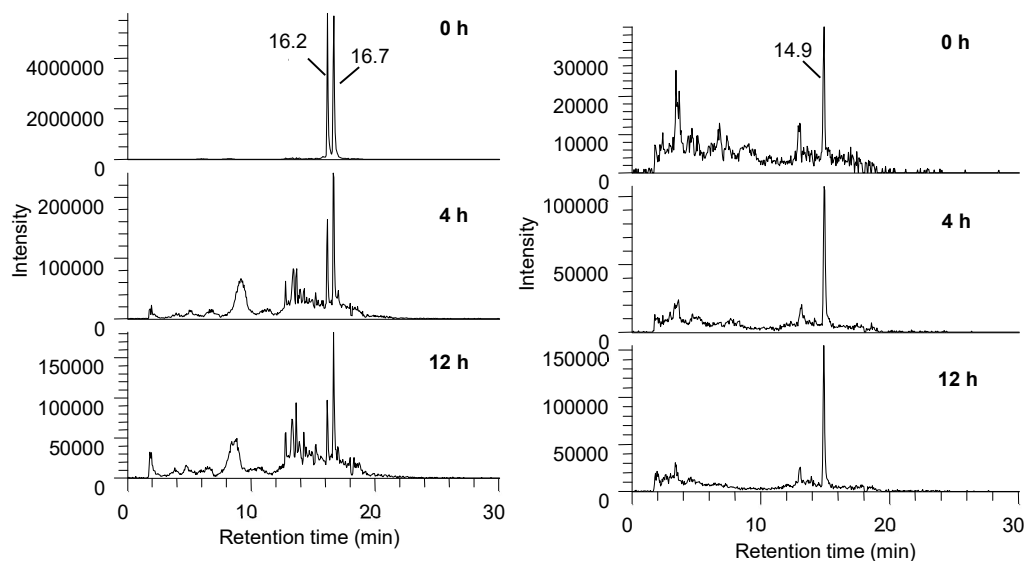
487 Guzman, 2017, Mekic et al., 2018; Mekic et al., 2019), phenols (Sun et al., 2010), etc).  
488 The presence of these highly oxygenated compounds that possibly contain acidic  
489 groups (e.g., –COOH and –OH) undoubtedly contributed to the increase of the solution  
490 acidity. Higher levels of other highly oxygenated species such as  $[C_3H_5O_3]^-$ ,  $[C_4H_7O_2]^-$ ,  
491  $[C_5H_5O_5]^-$  and  $[C_5H_7O_5]^-$  were also observed (Figure S9).

492 To identify the impact of photolysis on the evolution of specific WSOC, the ions of  
493  $[C_7H_7O_n]^-$  in the HBDM-1 sample with significant variation were chosen as  
494 representative cases for description. The relative intensity of  $[C_7H_7O_2]^-$  and  $[C_7H_7O_3]^-$   
495 decreased dramatically, while the intensities of  $[C_7H_7O_4]^-$ ,  $[C_7H_7O_5]^-$  and  $[C_7H_7O_6]^-$   
496 increased with the irradiation time (Figure 5 shows only the variation of  $[C_7H_7O_2]^-$  and  
497  $[C_7H_7O_4]^-$  as an example). It seems reasonable that the possible hydroxylation of  
498  $[C_7H_7O_2]^-$  and  $[C_7H_7O_3]^-$  might contribute to the formation of  $[C_7H_7O_5]^-$  and  $[C_7H_7O_6]^-$ .  
499 Although we could not verify this hypothesis, the formed oxidized species undoubtedly  
500 have a high O/C which highlights the possibility of this reaction pathway.

### 501 **3.4.2 Presentation of photochemically stable organic species**

502 Some of the detected organic species seemed to exhibit a good photochemical  
503 stability, as their relative intensities only slightly decreased (<10%) after 12h light  
504 irradiation. The m/z 161.0454 ( $[C_6H_9O_5]^-$ ) presented two prominent peaks at RT1.9 and  
505 2.4 min (Figure S10). The peak at RT 2.4 min was further confirmed with a standard  
506 compound to be levoglucosan, a typical tracer of biomass burning aerosols with a high  
507 photochemical stability in atmospheric aerosols (Hu et al., 2013). The relatively good  
508 photochemical stability was also observed for some  $C_6$  homolog compounds, such as

509  $[C_6H_7O_6]^-$ ,  $[C_6H_9O_6]^-$ , and  $[C_6H_{11}O_6]^-$ . Some other oxygenated species, such as  
510  $[C_3H_3O_3]^-$ ,  $[C_4H_5O_4]^-$ ,  $[C_3H_3O_4]^-$ , and  $[C_4H_5O_5]^-$  remained relatively stable, as well.



511

512 **Figure 5. Extracted LC chromatograms from HBDM-1 of (a)  $[C_7H_7O_2]^-$  and (b)  $[C_7H_7O_4]^-$  at**  
513 **different photolytic stages of 0, 4, and 12 h.**

514 Regarding the CHON compounds, only small variation of the chromatogram peaks,  
515 was observed for most of the detected species. In particular, several species with low  
516 O/C decreased by less than 30%, e.g.,  $m/z$  94.0297 ( $[C_5H_4ON]^-$ , RT 7.1 min), and  
517 120.0453 ( $[C_7H_6ON]^-$ , RT 12.2 min). Some compounds seem photochemically very  
518 stable as the variation of their peak intensities was less than 10 % upon light irradiation  
519 of the samples, e.g.,  $m/z$  118.0297 ( $[C_7H_4ON]^-$ , RT 16.6 and 17.1 min), 146.0246  
520 ( $[C_8H_4O_2N]^-$ , RT 14.4 min), and 190.0510 ( $[C_{10}H_8O_3N]^-$ , RT 17.8 min). However, the  
521 intensities of the ion masses with relatively higher degree of oxygenation was found to  
522 increase substantially (>50%), e.g.,  $m/z$  162.0195 ( $[C_8H_4O_3N]^-$ , RT 17.2 min), 198.0408  
523 ( $[C_8H_8O_5N]^-$ , RT 18.0 min), and 242.1763 ( $[C_{13}H_{24}O_3N]^-$ , RT 17.9 min). The  
524 photochemical stability of some compounds may be ascribed to their low

525 concentrations, or the light-shielding effect from other light-absorbing species.

526 Another intriguing finding was that different structural isomers with the same  
527 molecular mass might have exhibited different fates upon prolonged light irradiation of  
528 the samples. For example, the intensity of the peak at  $m/z$  165.0405 ( $[C_5H_9O_6]^-$ )  
529 decreased when it was eluted at 4.9 min, but increased at RT 1.8 min, with the  
530 irradiation time (Figure S11). A simultaneous degradation and formation among  
531 isomers of some CHON ion masses upon prolonged light irradiation, was also observed,  
532 as was the case for the CHO compounds. For example, the  $m/z$  108.0453 assigned to  
533  $[C_6H_6ON]^-$ , might include hydroxy and amino groups on the phenyl ring to present three  
534 possible isomers (Figure S12). During photolytic processing, the intensity of the peak  
535 at RT 3.2 min increased dramatically, while there was a clear decreasing tendency of  
536 the peak intensity at RT 5.5 and 12.5 min, which was suggestive of possible  
537 isomerization among these isomers. Other ion masses that exhibited possible  
538 isomerization included  $m/z$  122.0610 ( $[C_7H_8ON]^-$ ), 132.0454 ( $[C_8H_6ON]^-$ ), 134.0245  
539 ( $[C_7H_4O_2N]^-$ ), 136.0403 ( $[C_7H_6O_2N]^-$ ), 138.0559 ( $[C_7H_8O_2N]^-$ ), 144.0453 ( $[C_9H_6ON]^-$ ),  
540 and 152.0352 ( $[C_7H_6O_3N]^-$ ).

### 541 **3.4.3 Comparison of time-profile mass spectra of CHO composition in WSOC** 542 **extracts from WSBA samples**

543 Since the LC method just separated a fraction of polar compounds, we tentatively  
544 utilized the change of HRMS to gain more comprehensive information about the WSOC  
545 evolution. We compared the time-profile (0, 4, and 12h) mass spectra with each other,  
546 based on the assumption of same interference from inorganic species, and the good

547 reproducibility and stability for Orbitrap MS operated under the same instrumental  
548 parameters (the RSD of TIC intensity within 5%). It is well known that ESI mass  
549 spectral abundances are influenced by the solution composition, concentration of  
550 analytes and instrumental factors (Bateman et al., 2011); hence, it is quite challenging  
551 to directly quantify the absolute concentration levels of the complex mixtures. Despite  
552 that, the photochemical degradation of WSOC compounds and corresponding  
553 formation of organic compounds can be well described by the variation of signal  
554 intensity from mass spectrometry. The average O/C and H/C for CHO compounds were  
555 from  $0.38 \pm 0.02$  to  $0.44 \pm 0.02$  and  $1.24 \pm 0.03$  to  $1.26 \pm 0.01$ , respectively, as the  
556 irradiation time extended from 0 to 12h. The comparison of these time-profile mass  
557 spectra indicates that the 12-hour photolysis resulted in a significant reduction of  $28 \pm$   
558  $11\%$  in the total ion abundance (S/N). Since the photolysis induced changes in  
559 abundance for most of the CHO compounds, we also calculated the intensity (S/N)-  
560 weighted average O/C ( $O/C_w$ ) and H/C ( $H/C_w$ ) (Bateman et al., 2011; Romonosky et  
561 al., 2015) with values ranging from  $0.45 \pm 0.03$  to  $0.53 \pm 0.06$  and from  $1.32 \pm 0.09$  to  
562  $1.40 \pm 0.11$ , respectively. After the 12-h photolysis, both average H/C and  $H/C_w$  values  
563 slightly increased, compared to the samples prior to irradiation, however, both average  
564 O/C and  $O/C_w$  values have increased more distinctly, indicating an elevation in  
565 oxidation degree of bulk extract composition. This phenomenon could be partly  
566 reflected on the LC-HRMS observation, i.e. formation of highly oxygenated species  
567 and the consumption of low oxygenated compounds. In our previous study, the UV-VIS  
568 measurements revealed that the 12-h photochemical evolution leads to a modification

569 of absorptive properties for WSBA extracts (e.g., photo-bleaching at wavelengths  
570 below 380nm and photo-enhancement above 380nm) (Cai et al., 2018), which might be  
571 partially linked to present findings about molecular functionalization, e.g.,  
572 hydroxylation facilitating a red shift for light absorbing wavelengths.

#### 573 **4 CONCLUSIONS**

574 This study was focused on the effect of direct photolysis on the molecular  
575 composition of actual WSOC extracted from field straw-burning aerosol. The phenol  
576 dimer (m/z 185.0608) and guaiacol dimer (m/z 245.0823), or their isomers generated  
577 from laboratory aqueous-phase photooxidation of phenol and guaiacol were also  
578 observed in present field WSBA samples, suggesting that the aqueous phase reaction  
579 might contribute to the formation of emitted biomass burning aerosols. The laboratory  
580 observation on aqueous photochemistry of phenols indicated that those phenolic  
581 compounds in real biomass burning aerosols would likely have potential to experience  
582 similar evolution to form various oxygenated compounds under relevant atmospheric  
583 water conditions. The direct photolysis on the molecular composition of WSOC extracts  
584 from WSBA samples were performed to gain more insight into the evolution of aerosol  
585 composition. Because the extract composition was very complex, the techniques (ESI-  
586 HRMS and LC/ESI-HRMS) used in this study, although advanced still had limitations  
587 in monitoring the modification of molecular composition, especially for determining  
588 the potential formation of compounds present at low concentrations or compounds that  
589 were poorly ionized. However, a series of polar molecules were identified that changed  
590 their molecular composition via photochemical aging. In particular, the degradation of

591 low oxygenated compounds with strong photochemical reactivity and the formation of  
592 high oxygenated compounds might directly result in an increasing O/C in WSOC  
593 composition, which was likely linked to the modification of light-absorbing  
594 characteristics for extracts in previous study. This finding indicates that the water  
595 soluble organic fraction of field combustion-derived aerosols has the potential to form  
596 more oxidized organic matter, which might contribute to the highly oxygenated nature  
597 of atmospheric organic aerosols. Further studies focused on the photochemical  
598 evolution of WSOC composition will be performed in the future, including enlarging  
599 measurements on compound species (e.g., applying positive ESI-HRMS), identifying  
600 biomarkers and evaluating their role in photochemical processes.

#### 601 **AUTHOR CONTRIBUTION**

602 Jing Cai and Zhiqiang Yu designed the experiments, and Jing Cai and Xiangying Zeng  
603 carried them out. Guorui Zhi provided the straw-burning aerosol samples, Zhiqiang Yu  
604 and Sasho Gligorovski helped to perform the analysis of light irradiation and editing  
605 the manuscript. Guoying Sheng, Xinming Wang and Ping'an Peng provided some  
606 technical consultations about organic chemistry. Jing Cai prepared the manuscript with  
607 contributions from all co-authors.

#### 608 **ACKNOWLEDGMENTS**

609 This study was financially supported by the National Key Technology Research and  
610 Development Program of the Ministry of Science and Technology of China  
611 (2014BAC22B04), the National Natural Science Foundations of China (41225013,

612 41530641, 41373131, 41773131, and 41977187) and the Science and Technology  
613 Project of Guangdong Province, China (2014B030301060). We are grateful to  
614 Guangdong Foundation for Program of Science and Technology Research, Grant N°:  
615 2017B030314057.

## 616 REFERENCES

- 617 Altieri, K. E., Seitzinger, S. P., Carlton, A. G., Turpin, B. J., Klein, G. C. and Marshall, A. G.: Oligomers  
618 formed through in-cloud methylglyoxal reactions: Chemical composition, properties, and  
619 mechanisms investigated by ultra-high resolution FT-ICR mass spectrometry. *Atmospheric*  
620 *Environment*, 42, 1476-1490, 2008.
- 621 Altieri, K. E., Turpin, B. J. and Seitzinger, S. P.: Oligomers, organosulfates, and nitrooxy organosulfates  
622 in rainwater identified by ultra-high resolution electrospray ionization FT-ICR mass spectrometry,  
623 *Atmospheric Chemistry and Physics*, 9, 2533-2542, 2009a.
- 624 Altieri, K. E., Turpin, B. J. and Seitzinger, S. P.: Composition of Dissolved Organic Nitrogen in  
625 Continental Precipitation Investigated by Ultra-High Resolution FT-ICR Mass Spectrometry,  
626 *Environmental Science & Technology*, 43, 6950-6955, doi: 10.1021/es9007849, 2009b.
- 627 Anastasio, C., Faust, B. C. and Rao, C. J.: Aromatic carbonyl compounds as aqueous-phase  
628 photochemical sources of hydrogen peroxide in acidic sulfate aerosols, fogs, and clouds .1. Non-  
629 phenolic methoxybenzaldehydes and methoxyacetophenones with reductants (phenols),  
630 *Environmental Science & Technology*, 31, 218-232, 1997.
- 631 Bateman, A. P., Nizkorodov, S. A., Laskin, J. and Laskin, A.: Photolytic processing of secondary organic  
632 aerosols dissolved in cloud droplets, *Physical Chemistry Chemical Physics*, 13, 12199-12212, doi:  
633 10.1039/c1cp20526a, 2011.
- 634 Boone, E. J., Laskin, A., Laskin, J., Wirth, C., Shepson, P. B., Stirm, B. H. and Pratt, K. A.: Aqueous  
635 Processing of Atmospheric Organic Particles in Cloud Water Collected via Aircraft Sampling,  
636 *Environmental Science & Technology*, 49, 8523-8530, doi: 10.1021/acs.est.5b01639, 2015.
- 637 Cai, J., Zhi, G., Yu, Z., Nie, P., Gligorovski, S., Zhang, Y., Zhu, L., Guo, X., Li, P., He, T., He, Y.,  
638 Sun, J. and Zhang, Y.: Spectral changes induced by pH variation of aqueous extracts derived from



639 biomass burning aerosols: Under dark and in presence of simulated sunlight irradiation,  
640 Atmospheric Environment, 185, 1-6, doi: 10.1016/j.atmosenv.2018.04.037. 2018.

641 Cappiello, A., De Simoni, E., Fiorucci, C., Mangani, F., Palma, P., Truffelli, H., Decesari, S., Facchini, M.  
642 C. and Fuzzi, S.: Molecular characterization of the water-soluble organic compounds in fogwater  
643 by ESIMS/MS, Environmental Science & Technology, 37, 1229-1240, doi: 10.1021/es0259990,  
644 2003.

645 Chang, J. L. and Thompson, J. E.: Characterization of colored products formed during irradiation of  
646 aqueous solutions containing H<sub>2</sub>O<sub>2</sub> and phenolic compounds, Atmospheric Environment, 44, 541-  
647 551, doi: 10.1016/j.atmosenv.2009.10.042, 2010.

648 Carlton, A. G., Turpin, B. J., Altieri, K. E., Seitzinger, S., Reff, A., Lim, H-J. and Ervens, B.: Atmospheric  
649 oxalic acid and SOA production from glyoxal: Results of aqueous photooxidation experiments.  
650 Atmospheric Environment, 41, 7588–7602, 2007.

651 Collett, J.L., Hoag, K.J., Sherman, D.E., Aaron Bator; Richards, W.L. Spatial and temporal variations in  
652 San Joaquin Valley fog chemistry, Atmospheric Environment, 33 (1), 129-140, 1998.Daumit, K. E.,  
653 Carrasquillo, A. J., Hunter, J. F. and Kroll, J. H.: Laboratory studies of the aqueous-phase oxidation  
654 of polyols: submicron particles vs. bulk aqueous solution, Atmospheric Chemistry and Physics, 14,  
655 10773-10784, doi: 10.5194/acp-14-10773-2014, 2014.

656 Duarte, R. M. B. O., Santos, E. B. H., Pio, C. A. and Duarte, A. C.: Comparison of structural features of  
657 water-soluble organic matter from atmospheric aerosols with those of aquatic humic substances,  
658 Atmospheric Environment, 41, 8100-8113, doi: 10.1016/j.atmosenv.2007.06.034, 2007.

659 Eugene, A. J. and Guzman, M. I. Reactivity of Ketyl and Acetyl Radicals from Direct Solar Actinic  
660 Photolysis of Aqueous Pyruvic Acid. Journal of Physical Chemistry A, 121, 2924–2935, 2017.

661 Fahey, K. M., Pandis, S. N., Collett, J. L. and Herckes, P. The influence of size-dependent droplet  
662 composition on pollutant processing by fogs, Atmospheric Environment, 39(25), 4561-4574, 2005.

663 Fine, P. M., Cass, G. R. and Simoneit, B. R. T.: Chemical characterization of fine particle emissions from  
664 fireplace combustion of woods grown in the northeastern United States, Environmental Science &  
665 Technology, 35, 2665-2675, 2001.

666 Fu, P. Q., Kawamura, K., Chen, J., Qin, M. Y., Ren, L. J., Sun, Y. L., Wang, Z. F., Barrie, L. A., Tachibana,  
667 E., Ding, A. J. and Yamashita, Y.: Fluorescent water-soluble organic aerosols in the High Arctic  
668 atmosphere, Scientific Reports, 5, 2015.

669 Gilardoni, S., Massoli, P., Paglione, M., Giulianelli, L., Carbone, C., Rinaldi, M., Decesari, S., Sandrini,  
670 S., Costabile, F., Gobbi, G. P., Pietrogrande, M. C., Visentin, M., Scotto, F., Fuzzi, S. and Facchini,  
671 M. C.: Direct observation of aqueous secondary organic aerosol from biomass-burning emissions,  
672 Proceedings of the National Academy of Sciences of the United States of America, 113, 10013-  
673 10018, 2016.

674 Gómez Alvarez, E., Wortham, H., Streckowski, R., Zetzsch, C., S. Gligorovski, S.: Atmospheric photo-  
675 sensitized heterogeneous and multiphase reactions: From outdoors to indoors, Environmental  
676 Science & Technology, 46, 1955-1963, 2012.

677 Graham, B., Mayol-Bracero, O. L., Guyon, P., Roberts, G. C., Decesari, S., Facchini, M. C., Artaxo, P.,  
678 Maenhaut, W., Koll, P. and Andreae, M. O.: Water-soluble organic compounds in biomass burning  
679 aerosols over Amazonia-1. Characterization by NMR and GC-MS, Journal of Geophysical  
680 Research-Atmospheres, 107, doi: 10.1029/2001jd000336, 2002.

681 Grgic, I., Nieto-Gligorovski, L.I., Net, S., Temime-Roussel, B., Gligorovski, S. and Wortham, H.: Light  
682 induced multiphase chemistry of gas-phase ozone on aqueous pyruvic and oxalic acids, Physical  
683 Chemistry Chemical Physics, 12, 698-707, 2010.

684 Griffith, E. C., Carpenter, B. K., Shoemaker, R. K. and Vaida, V.: Photochemistry of aqueous pyruvic  
685 acid, Proceedings of the National Academy of Sciences of the United States of America, 110, 11714-  
686 11719, doi: 10.1073/pnas.1303206110, 2013.

687 Hu, Q., Xie, Z., Wang, X., Hui Kang, H. and Zhang, P.: Levoglucosan indicates high levels of biomass  
688 burning aerosols over oceans from the Arctic to Antarctic, Scientific Reports, 3, 2013.

689 Kitanovski, Z., Cusak, A., Grgic, I. and Claeys, M.: Chemical characterization of the main products  
690 formed through aqueous-phase photonitration of guaiacol, Atmospheric Measurement Techniques, 7,  
691 2457-2470, doi: 10.5194/amt-7-2457-2014, 2014.

692 Kroll, J. H., Donahue, N. M., Jimenez, J. L., Kessler, S. H., Canagaratna, M. R., Wilson, K. R., Altieri, K.  
693 E., Mazzoleni, L. R., Wozniak, A. S., Bluhm, H., Mysak, E. R., Smith, J. D., Kolb, C. E., and Worsnop,  
694 D. R.: Carbon oxidation state as a metric for describing the chemistry of atmospheric organic aerosol,  
695 Nat. Chem. Biol., 3, 133-139, 2011.

696 Kourchev, I., Fuller, S., Aalto, J., Ruuskanen, T. M., McLeod, M. W., Maenhaut, W., Jones, R., Kulmala,  
697 M. and Kalberer, M.: Molecular Composition of Boreal Forest Aerosol from Hyytiälä, Finland,  
698 Using Ultrahigh Resolution Mass Spectrometry, Environmental Science & Technology, 47, 4069-

699 4079, doi: 10.1021/es3051636, 2013.

700 Kourtchev, I., Godoi, R. H. M., Connors, S., Levine, J.G., Archibald, A.T., Godoi, A. F. L., Paralovo,  
701 S.L., Barbosa, C. G. G., Souza, R. A. F., Manzi, A. O., Seco, R., Sjöstedt, S., Park, J. H., Guenther  
702 A., Kim, S., Smith, J., Martin, S. T., and Kalberer, M.: Molecular composition of organic aerosols  
703 in central Amazonia: an ultra-high-resolution mass spectrometry study, *Atmospheric Chemistry  
704 and Physics*, 16, 11899–11913, 2016.

705 Krivacsy, Z., Hoffer, A., Sarvari, Z., Temesi, D., Baltensperger, U., Nyeki, S., Weingartner, E., Kleefeld,  
706 S. and Jennings, S. G.: Role of organic and black carbon in the chemical composition of atmospheric  
707 aerosol at European background sites, *Atmospheric Environment*, 35, 6231–6244, 2001.

708 Laskin, A., Smith, J. S. and Laskin, J.: Molecular Characterization of Nitrogen-Containing Organic  
709 Compounds in Biomass Burning Aerosols Using High-Resolution Mass Spectrometry,  
710 *Environmental Science & Technology*, 43, 3764–3771, doi: 10.1021/es803456n, 2009.

711 Lavi, A., Lin, P., Bhaduri, B., Carmieli, R., Laskin, A. and Rudich, Y.: Characterization of light-absorbing  
712 oligomers from reactions of phenolic compounds and Fe(III), *Earth and Space Chemistry*, 1, 637–646,  
713 2017.

714 Lee, A. K. Y., Herckes, P., Leaitch, W. R., Macdonald, A. M. and Abbatt, J. P. D.: Aqueous OH oxidation  
715 of ambient organic aerosol and cloud water organics: Formation of highly oxidized products,  
716 *Geophysical Research Letters*, 38, 2011.

717 Lim, Y. B., Tan, Y., Perri, M. J., Seitzinger, S. P. and Turpin, B. J.: Aqueous chemistry and its role in  
718 secondary organic aerosol (SOA) formation, *Atmospheric Chemistry and Physics*, 10, 10521–10539,  
719 doi: 10.5194/acp-10-10521-2010, 2010.

720 Lim, Y. B. and Turpin, B. J.: Laboratory evidence of organic peroxide and peroxyhemiacetal formation  
721 in the aqueous phase and implications for aqueous OH, *Atmospheric Chemistry and Physics*, 15,  
722 12867–12877, doi: 10.5194/acp-15-12867-2015, 2015.

723 Lin, P., Rincon, A. G., Kalberer, M. and Yu, J. Z.: Elemental Composition of HULIS in the Pearl River  
724 Delta Region, China: Results Inferred from Positive and Negative Electrospray High Resolution  
725 Mass Spectrometric Data, *Environmental Science & Technology*, 46, 7454–7462, doi:  
726 10.1021/es300285d, 2012a.

727 Lin, P., Yu, J. Z., Engling, G. and Kalberer, M.: Organosulfates in Humic-like Substance Fraction Isolated  
728 from Aerosols at Seven Locations in East Asia: A Study by Ultra-High-Resolution Mass

729 Spectrometry, *Environmental Science & Technology*, 46, 13118-13127, doi: 10.1021/es303570v,  
730 2012b.

731 Mayol-Bracero, O. L., Guyon, P., Graham, B., Roberts, G., Andreae, M. O., Decesari, S., Facchini, M.  
732 C., Fuzzi, S. and Artaxo, P.: Water-soluble organic compounds in biomass burning aerosols over  
733 Amazonia - 2. Apportionment of the chemical composition and importance of the polyacidic  
734 fraction, *Journal of Geophysical Research-Atmospheres*, 107, doi: 10.1029/2001jd000522, 2002.

735 McNeill, V. F.: Aqueous Organic Chemistry in the Atmosphere: Sources and Chemical Processing of  
736 Organic Aerosols, *Environmental Science & Technology*, 49, 1237-1244, 2015.

737 Mekic, M., Loisel, G., Zhou, W., Jiang, B., Vione, D., Gligorovski, S.: Ionic strength effects on the reactive  
738 uptake of ozone on aqueous pyruvic acid: Implications for air-sea ozone deposition, *Environmental  
739 Science and Technology*, 52, 12306–12315, 2018.

740 Mekic, M., Liu, J., Zhou, W., Loisel, G., Cai, J., He, T., Jiang, B., Yu, Z., Lazarou, Y. G., Li, X., Brigante,  
741 M., Vione, D., Gligorovski, S.: Formation of highly oxygenated multifunctional compounds from  
742 cross-reactions of carbonyl compounds in the atmospheric aqueous phase, *Atmospheric  
743 Environment*, 219, 117046, 2019.

744 Net, S., Nieto-Gligorovski, L., Gligorovski, S., Temime-Roussel, B., Barbati, S., Lazarou, Y. G., and  
745 Wortham, H.: Heterogeneous light induced ozone processing on the organic coatings in the  
746 atmosphere, *Atmospheric Environment*, 43, 1683-1692, 2009.

747 Net, S., Nieto-Gligorovski, L., Gligorovski, S., and Wortham, H.: Heterogeneous ozonation kinetics of 4-  
748 phenoxyphenol in presence of photosensitizer, *Atmospheric Chemistry and Physics*, 10, 1545-1554,  
749 2010b.

750 Net, S., Gligorovski, S., and Wortham, H.: Light-induced heterogeneous ozone processing on organic  
751 coated particles: Kinetics and condensed-phase products, *Atmospheric Environment*, 44, 3286-3294,  
752 2010b.

753 Nguyen, T. B., Lee, P. B., Updyke, K. M., Bones, D. L., Laskin, J., Laskin, A. and Nizkorodov, S. A.:  
754 Formation of nitrogen- and sulfur-containing light-absorbing compounds accelerated by  
755 evaporation of water from secondary organic aerosols, *Journal of Geophysical Research-  
756 Atmospheres*, 117, doi: 10.1029/2011jd016944, 2012.

757 Ofner, J., Krueger, H. U., Grothe, H., Schmitt-Kopplin, P., Whitmore, K. and Zetzsch, C.: Physico-  
758 chemical characterization of SOA derived from catechol and guaiacol - a model substance for the

759 aromatic fraction of atmospheric HULIS, *Atmospheric Chemistry and Physics*, 11, 1-15, doi:  
760 10.5194/acp-11-1-2011, 2011.

761 Petzold, A., Kopp, C., Niessner, R., 1997. The dependence of the specific attenuation cross-section on  
762 black carbon mass fraction and particle size. *Atmospheric Environment*, 31, 661-672, 1997.

763 Prasse, C., Ford, B., Nomura, D.K. and Sedlak, D.L.: Unexpected transformation of dissolved phenols  
764 to toxic dicarbonyls by hydroxyl radicals and UV light, <https://doi.org/10.1073/pnas.1715821115>,  
765 2018.

766 Rapf, R. J., Perkins, R. J., Carpenter, B. K. and Vaida, V.: Mechanistic Description of Photochemical  
767 Oligomer Formation from Aqueous Pyruvic Acid. *Journal of Physical Chemistry A*, 121, 4272–4282,  
768 2017.

769 Reed Harris, A. E., Ervens, B., Shoemaker, R. K., Kroll, J. A., Rapf, R. J., Griffith, E. C., Monod, A.,  
770 Vaida, V.: Photochemical kinetics of pyruvic acid in aqueous solution. *Journal of Physical  
771 Chemistry A*, 118 (37), 8505–8516, 2014.

772 Romonosky, D. E., Laskin, A., Laskin, J. and Nizkorodov, S. A.: High-Resolution Mass Spectrometry  
773 and Molecular Characterization of Aqueous Photochemistry Products of Common Types of  
774 Secondary Organic Aerosols, *Journal of Physical Chemistry A*, 119, 2594-2606, doi:  
775 10.1021/jp509476r, 2015.

776 Rossignol, S., Aregahegn, K. Z., Tinel, L., Fine, L., Noziere, B. and George, C.: Glyoxal Induced  
777 Atmospheric Photosensitized Chemistry Leading to Organic Aerosol Growth, *Environmental  
778 Science & Technology*, 48, 3218-3227, 2014.

779 Simoneit, B. R. T.: Biomass burning - A review of organic tracers for smoke from incomplete combustion,  
780 *Applied Geochemistry*, 17, 129-162, doi: 10.1016/s0883-2927(01)00061-0, 2002.

781 Smith, J. D., Sio, V., Yu, L., Zhang, Q. and Anastasio, C.: Secondary Organic Aerosol Production from  
782 Aqueous Reactions of Atmospheric Phenols with an Organic Triplet Excited State, *Environmental  
783 Science & Technology*, 48, 1049-1057, doi: 10.1021/es4045715, 2014.

784 Smith, J. S., Laskin, A. and Laskin, J.: Molecular Characterization of Biomass Burning Aerosols Using  
785 High-Resolution Mass Spectrometry, *Analytical Chemistry*, 81, 1512-1521, doi: 10.1021/ac8020664,  
786 2009.

787 Smith, J. D., Kinney, H. and Anastasio, C.: Phenolic carbonyls undergo rapid aqueous photodegradation  
788 to form low-volatility, light-absorbing products, *Atmospheric environment*, 126, 36-44, 2015.

789 Sun, Y. L., Zhang, Q., Anastasio, C. and Sun, J.: Insights into secondary organic aerosol formed via  
790 aqueous-phase reactions of phenolic compounds based on high resolution mass spectrometry,  
791 Atmospheric Chemistry and Physics, 10, 4809-4822, doi: 10.5194/acp-10-4809-2010, 2010.

792 Surratt, J. D., Gomez-Gonzalez, Y., Chan, A. W. H., Vermeylen, R., Shahgholi, M., Kleindienst, T. E.,  
793 Edney, E. O., Offenberg, J. H., Lewandowski, M., Jaoui, M., Maenhaut, W., Claeys, M., Flagan, R.  
794 C. and Seinfeld, J. H.: Organosulfate formation in biogenic secondary organic aerosol, Journal of  
795 Physical Chemistry A, 112, 8345-8378, doi: 10.1021/jp802310p, 2008.

796 Surratt, J. D., Kroll, J. H., Kleindienst, T. E., Edney, E. O., Claeys, M., Sorooshian, A., Ng, N. L.,  
797 Offenberg, J. H., Lewandowski, M., Jaoui, M., Flagan, R. C. and Seinfeld, J. H.: Evidence for  
798 organosulfates in secondary organic aerosol, Environmental Science & Technology, 41, 517-527, doi:  
799 10.1021/es062081q, 2007.

800 Tong, H., Kourtchev, I., Pant, P., Keyte, I. J., O'Connor, I. P., Wenger, J. C., Pope, F. D., Harrison, R. M.  
801 and Kalberer, M.: Molecular composition of organic aerosols at urban background and road tunnel  
802 sites using ultra-high resolution mass spectrometry. Faraday Discussions, 189, 51-68, 2016.

803 Vione, D., Maurino, V., Minero, C., Pelizzetti, E., Harrison, M. A. J., Olariu, R. I. and Arsene, C.:  
804 Photochemical reactions in the tropospheric aqueous phase and on particulate matter, Chemical  
805 Society Reviews, 35, 441-453, 2006.

806 Vione, V., Albinet, A., Barsotti, F., Mekic, M., Jiang, B., Minero, C., Brigante, M., Gligorovski, S.:  
807 Formation of substances with humic-like fluorescence properties, upon photoinduced  
808 oligomerization of typical phenolic compounds emitted by biomass burning, Atmospheric  
809 Environment, <https://doi.org/10.1016/j.atmosenv.2019.03.005>, 2019.

810 Wang, X. K., Rossignol, S., Ma, Y., Yao, L., Wang, M. Y., Chen, J. M., George, C. and Wang, L.:  
811 Molecular characterization of atmospheric particulate organosulfates in three megacities at the  
812 middle and lower reaches of the Yangtze River, Atmospheric Chemistry and Physics, 16, 2285-2298,  
813 2016.

814 Wang, X., Hayeck, N., Brüggemann, M., Yao, L., Chen, H., Zhang, C., Emmelin, C., Jianmin Chen, J.,  
815 George, C. and Lin Wang, L. Chemical characteristics of organic aerosols in shanghai: A study by  
816 ultrahigh-performance liquid chromatography coupled with Orbitrap mass spectrometry, Journal of  
817 Geophysical Research-Atmospheres, 122 (11), 703-722, 2017.

818 Wozniak, A. S., Bauer, J. E., Sleighter, R. L., Dickhut, R. M. and Hatcher, P. G.: Technical Note:

819 Molecular characterization of aerosol-derived water soluble organic carbon using ultrahigh  
820 resolution electrospray ionization Fourier transform ion cyclotron resonance mass spectrometry,  
821 Atmospheric Chemistry and Physics, 8, 5099-5111, 2008.

822 Xie, M. J., Mladenov, N., Williams, M. W., Neff, J. C., Wasswa, J. and Hannigan, M. P.: Water soluble  
823 organic aerosols in the Colorado Rocky Mountains, USA: composition, sources and optical  
824 properties, Scientific Reports, 6, 2016.

825 Yee, L. D., Kautzman, K. E., Loza, C. L., Schilling, K. A., Coggon, M. M., Chhabra, P. S., Chan, M. N.,  
826 Chan, A. W. H., Hersey, S. P., Crounse, J. D., Wennberg, P. O., Flagan, R. C. and Seinfeld, J. H.:  
827 Secondary organic aerosol formation from biomass burning intermediates: phenol and  
828 methoxyphenols, Atmospheric Chemistry and Physics, 13, 8019-8043, 2013.

829 Yu, L., Smith, J., Laskin, A., Anastasio, C., Laskin, J. and Zhang, Q.: Chemical characterization of SOA  
830 formed from aqueous-phase reactions of phenols with the triplet excited state of carbonyl and  
831 hydroxyl radical, Atmospheric Chemistry and Physics, 14, 13801-13816, doi: 10.5194/acp-14-  
832 13801-2014, 2014.

833 Zhao, Y., Hallar, A. G. and Mazzoleni, L. R.: Atmospheric organic matter in clouds: exact masses and  
834 molecular formula identification using ultrahigh-resolution FT-ICR mass spectrometry,  
835 Atmospheric Chemistry and Physics, 13, 12343-12362, doi: 10.5194/acp-13-12343-2013, 2013.

836 Zhi, G., Chen, Y., Xue, Z., Meng, F., Cai, J., Sheng, G. and Fu, J.: Comparison of elemental and black  
837 carbon measurements during normal and heavy haze periods: implications for research,  
838 Environmental Monitoring and Assessment, 186, 6097-6106, doi: 10.1007/s10661-014-3842-2,  
839 2014.

840 Zhou, W., Mekic, M., Liu, J., Loisel, G., Jin, B., Vione, D., Gligorovski, S.: Ionic strength effects on the  
841 photochemical degradation of acetosyringone in atmospheric deliquescent aerosol particles,  
842 Atmospheric Environment, 198, 83-88, 2019.